Chemistry–A European Journal
Communication
doi.org/10.1002/chem.202102031

Chemistry Europe
European Chemical Societies Publishing

Electrocatalytic H_2 Generation from Water Relying on Cooperative Ligand Electron Transfer in "PN^{3}P" Pincer-Supported Ni^{II} Complexes

Somayeh Norouziyanlakvan,[a] Gyandshwar Kumar Rao,[a] Jeffrey Ovens,[a] Bulat Gabidullin,[a] and Darrin Richeson*[a]

Abstract: Water is the most sustainable source for H_2 production, and the efficient electrocatalytic production of H_2 from mixed water/acetonitrile solutions by using two new air-stable nickel(II) pincer complexes, [Ni(κ^3-2,6-{Ph_2PNR}$_2$(NC_5H_3)Br_2] (R = H **I**, Me **II**) is reported. Hydrogen generation from H_2O/CH_3CN solutions is initiated at −2 V against Fc$^{+/0}$, and bulk electrocatalysis studies showed that the catalyst functions with an excellent Faradaic efficiency and a turnover frequency of 160 s^{-1}. A DFT computational investigation of the reduction behavior of **I** and **II** revealed a correlation of H_2 formation with charge donation from electrons originating in a reduced ligand-localized orbital. As a result, these catalysts are proposed to proceed by a novel mechanism involving electron/proton transfer between a Ni^{0I} species bonded to an anionic PN^{3}P ligand ("L$^-$/Ni^{0I}") and a Ni^I-hydride ("Ni–H"). Furthermore, these catalysts are able to reduce phenol and acetic acid, more active proton sources, at lower potentials that correlate with the substrate pK_a.

Dihydrogen, the simplest of molecules, represents an ideal, environmentally innocent energy source that affords water as the sole product of oxidation. In order to enable a sustainable production of H_2, it is crucial to discover and interrogate electrocatalysts based on earth-abundant metals. Furthermore, water represents the optimal substrate for the generation of hydrogen and viable catalytic processes directly using water as the hydrogen source are desirable.

The report that tetraazamacrocycle (cyclam) complexes of Co and Ni were capable of generating H_2 from neutral water under electrochemical conditions was a starting point for discovery of a wide range of metal complexes that can reduce protons to hydrogen.[1–5] The majority of these species perform in polar organic solvents and require the presence of acids as a hydrogen source even with electrocatalysis in aqueous solution. In general, complexes that are capable of catalyzing hydrogen evolution from simple water as a source are still rare.[2–5] While many of these reports focus on the important performance parameters of the acid-based catalysis, the lower environmental and economic impacts as well as revealing fundamental features that would allow use of water as a substrate clearly inspires attention and motivates discovery of new earth-abundant catalysts and mechanisms.

Nickel is an attractive metal center for designing new H_2 generation catalysts due to its abundance and ability to form complexes with a range of accessible oxidation states and flexible coordination behavior.[4] Added stimulus comes from the appearance of Ni as a component in hydrogenase enzymes.[6] These features provide motivation to explore and design ligand scaffolds that would enable Ni complexes as hydrogen evolution catalysts. One particularly successful approach has been with ligands bearing pendant moieties (e.g., amines) as proton shuttles, which act cooperatively with the nickel center, as a hydride donor, for electrocatalytic proton reduction. For example, several well-known Ni^{II} phosphine complexes bear pendant proximal amines that provide a crucial role in electrocatalytic proton reduction.[4,7,8] Recently, redox non-innocent ligands have been shown to participate in ligand-based proton coupled electron transfer (PCET) for Ni-based proton reduction.[5,9] Some examples include, Ni^{II} dithiolate and nickel porphyrin electrocatalysts having ligand centered redox and proton transfer capabilities.[10–12] Remarkably, the concept of using redox active ligands for hydrogen evolution has been expanded to include metal-free thiosemicarbazone and redox inactive Zn^{II} complexes of this redox active species.[13,14] Notably, all of these examples employ acid as the proton/hydrogen source. Recently, complexes of Ni^{II} and *N*-benzyl-*N*,*N'*,*N'*-tris(2-pyridylmethyl)ethylenediamine ligands have been reported as efficient catalysts for H_2 evolution from water at −2.09 V against Fc$^{+/0}$.[15,16] This reduction was assigned to being between a Ni$^{I/0}$ reduction couple and a ligand centered reduction at −2.6 V.

Our efforts to reveal new Ni catalysts for the production of hydrogen from water began with the choice of *N*,*N'*-bis(diphenylphosphino)-2,6-diaminopyridine species (2,6-{Ph_2PNR}$_2$(NC_5H_3; R = H, Me) as ligands. These "PN^{3}P" neutral pincer ligands offer tunability of sterics and electronic properties and are known to support catalysts for variety of reactions.[17] In the case of R = H, the PN^{3}P ligand has been demonstrated to display non-innocence through deprotonation and "dearomatization" of the backbone during catalysis.[18–20]

---

[a] S. Norouziyanlakvan, Dr. G. K. Rao, Dr. J. Ovens, Dr. B. Gabidullin, Dr. D. Richeson
Department of Chemistry and Biomolecular Sciences
Centre for Catalysis Research and Innovation
University of Ottawa
10 Marie Curie, Ottawa, ON K1 N 6 N5
E-mail: darrin@uottawa.ca

Supporting information for this article is available on the WWW under https://doi.org/10.1002/chem.202102031

Furthermore, we have previously demonstrated PN^{3}P-supported Co complexes as efficient electrocatalysts for H_2 formation.[21]

We report two air-stable Ni^{II}-PN^{3}P pincer complexes that perform electrocatalytic hydrogen evolution from mixed water/acetonitrile solutions. We find, through a combination of empirical and computational observations that the PN^{3}P ligand acts an electron reservoir for this transformation.

Ready access to the PN^{3}P complexes of Ni^{II} was provided by direct reaction of the appropriate ligand and a suspension of anhydrous $NiBr_2$ (Figure 1). Complexes **I** and **II** were stable under ambient conditions and could be stored for months. NMR spectroscopic analysis indicated that both species possessed symmetrically coordinated ligands as exemplified by a single NMR resonance for the N–H groups, and symmetrical pyridyl and phenyl substituents in the ^{1}H NMR. Additionally, the ^{31}P NMR displayed a single resonance. These features were supported by single crystal X-ray analysis (Figures S1 and S2).

The structure of complex **I** consisted of the cationic complex $[Ni(2,6\text{-}\{Ph_2PNH\}_2(NC_5H_3)Br]^+$ (**1**$^+$) with a charge balancing bromide anion (Figure S1).The Ni^{II} center displayed a distorted square planar coordination geometry described by a planar, tridentate pincer PN^{3}P ligand and completed by a bromo ligand. The structure of **1**$^+$ compares favorably with the reported structures of $[Ni(2,6\text{-}\{Ph_2PNH\}_2(NC_5H_3)Cl]Cl$,[22] $[Ni(2,6\text{-}\{tBu_2PNH\}_2(NC_5H_3)Br]Br$[23] and $Ni(2,6\text{-}\{iPr_2PNH\}_2(NC_3N_2H_2(NMe_2))Cl]Cl$.[24] In contrast complex **II**, $[Ni(2,6\text{-}\{Ph_2PNMe\}_2(NC_5H_3)Br_2$, presented an asymmetric unit with a monomeric five-coordinate Ni^{II} with distorted square pyramidal geometry, an unprecedented geometry with the PN^{3}P ligand. The ligand was coordinated to Ni in a planar tridentate fashion through the nitrogen and two phosphorus centers, occupying three basal positions of the square pyramid. One bromo ligand, Br1, occupied the remaining basal position, *trans* to the pyridyl N center, with Br2 filling an apical position, perpendicular to this plane with the average angle between Br2 and the other four coordinated centers of 97.4°. This apical Br(2)-Ni(1) distance was much longer (2.7961(9) Å) than the basal Br(1)-Ni(1) length (2.3100(6) Å). Interestingly, this Ni(1)-Br(1) distance is similar to the analogous Ni–Br distance in complex **I** (2.2741(4) Å). Furthermore, the Ni–P bond distances in **II** (P(1)–Ni(1) 2.1432(9) Å, P(2)–Ni(1) 2.1687(9) Å) are similar to those in **I** (i.e., 2.1705(5) Å, 2.1686(5) Å) and the Ni(1)–N(2) distance 1.911(2) Å is slightly longer than the corresponding Ni–N distance in **I** at 1.8857(15) Å. These data suggest that **II** is related to **I** with an additional weak apical coordination of a bromide anion, Br(2), to Ni.

Cyclic voltammetric scans of **I** and **II** in dry acetonitrile, under cathodic potentials, are shown in Figure 2 (Figures S3–S5). All of these potential measurements were referenced to the reversible ferrocene couple ($Fc^{+/0}$, $\Delta E_p = 200$ mV). Both complexes exhibited similar profiles with three reduction events. The first was a reversible reduction at $E_{1/2} = -0.93$ V (**I**, $\Delta E_p = 160$ mV) and $E_{1/2} = -0.89$ V (**II**, $\Delta E_p = 160$ mV), respectively. A second reduction was irreversible at −1.4 (**I**) and −1.32 V (**II**). Both complexes displayed a third irreversible reduction at −2.49 (**I**) and −2.57 V (**II**). All of these reduction events displayed a linear dependence of the current intensity on the square root of the scan rate, consistent with freely diffusing species (Figures S6 and S7). The similarity of the electrochemical features of **I** and **II**, along with the structural features noted above, encouraged our investigation of these species by computation.

Significant insights into the electronic structure and proposed nature of the reduction behavior of **I** and **II** were delivered through a DFT computational investigation using the B3LYP functional and def2TZVP basis set and employing the IEFPCM model for solvation with acetonitrile. This investigation began with an optimization of the cation $[Ni(\kappa^3\text{-}2,6\text{-}\{Ph_2PNMe\}_2NC_5H_3)Br]^+$ (**1**$^+$) of **I**. The computational results for **1**$^+$ produced an excellent match with the experimental structure (Figures S8 and S9, Tables S5 and S6). Notably, the analogous optimization process on **II** in acetonitrile led to spontaneous dissociation of the apical Br^- to produce the analogue of **1**$^+$, $[Ni(\kappa^3\text{-}2,6\text{-}\{Ph_2PNMe\}_2NC_5H_3)Br]^+$ (**2**$^+$). The cation **2**$^+$ was optimized to yield a comparable structure of **1**$^+$ (Figure S17, Tables S10 and S11) and this is consistent with the observation of similar electrochemistry seen for the two Ni species. These structures form a starting point for exploring the reduction events for these two complexes and, as expected, both displayed distorted square planar d^8 Ni^{II} centers with filled Ni-centered d_{xy}, d_{xz}, d_{yz} and d_{z^2} σ nonbonding MOs and an

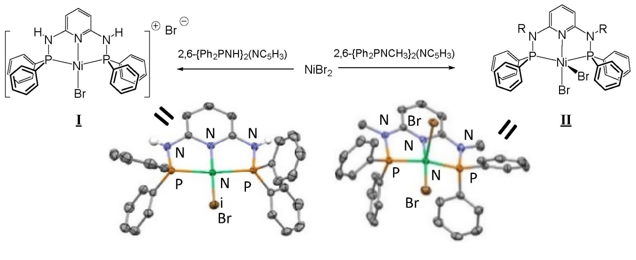

Figure 1. Reaction scheme and structures of complexes **1**$^+$ (complex **I** bromide counterion not shown) and **II**.

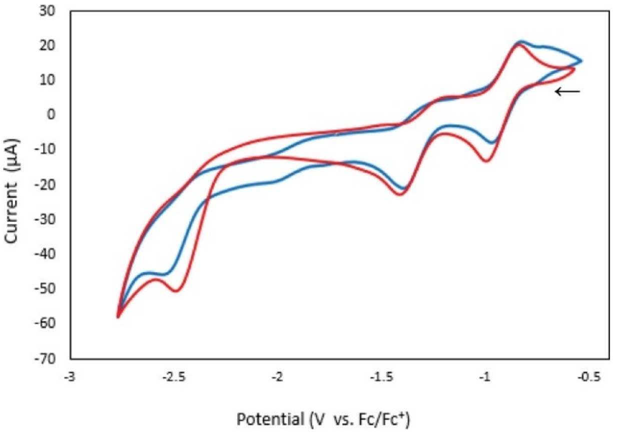

Figure 2. CV of complexes **I** (red) and **II** (blue; 1.0 mM) under N_2, in 0.1 M tetrabutylammonium hexafluorophosphate (TBAHFP) solution in CH_3CN and scan rate was 100 mV/s. The arrow indicates initial scan direction. (open circuit potential ca. −0.6 V).

empty $d_{x^2-y^2}$-centered σ* orbital as the LUMO (Figures S10 and S18)

By employing the same computational optimization parameters, we were able to obtain a logical and consistent set of structures for the sequential addition of three electrons to these cations. Focusing on $[Ni(\kappa^3\text{-}2,6\text{-}\{Ph_2PNMe\}_2NC_5H_3)Br]^+$ (**1**$^+$), addition of the first electron yielded a square planar neutral species (**1**) (Figures S11 and S12) where this electron was added to a $d_{x^2-y^2}$-based orbital to give a SOMO which displayed similar σ* character as seen in **1**$^+$. Mayer bond analysis indicated an overall decrease in bond order compared with **1**$^+$ with the largest effect on Ni–Br. As a result, we interpret the first reduction wave as a Ni^{II}/Ni^{I} couple. The addition of the next electron converted **1** to **1**$^-$. This electron was again added to the orbital with $d_{x^2-y^2}$ character (Figures S13 and S14) and thus we assigned this irreversible wave to a Ni^{I}/Ni^{0I} couple and complex **1**$^-$ as an 18 electron species. By filling the σ* MO, not surprisingly, this reduction produced an optimized structure with substantial changes that included deviation of the Ni^{0I} center from square planar geometry, an increase in Ni–Br bond length and decrease in bond order (Table S8). Finally, the addition of an electron to **1**$^-$, led to a spontaneous and anticipated loss of bromide anion to yield a planar T-shaped complex $[Ni(\kappa^3\text{-}2,6\text{-}\{Ph_2PNH\}_2NC_5H_3)]^-$ (**A**$^-$; Figure S15). Examination of the electronic structure of this anion confirmed four Ni-centered d_{xz}, d_{z^2}, d_{xz}, d_{xy} occupied orbitals that were essentially nonbonding and an occupied σ* orbital that was about 70 % Ni $d_{x^2-y^2}$ in character (Figure S16). The additional electron was determined to reside in a ligand localized SOMO that was about equally dispersed on the ligand P centers and py moiety with less than 10 % of the density on Ni as shown in Figure 3. Following this process with the analogous complex **2+** led to a parallel set of results at each reduction step (Figures S17–S22, Tables S10–S13).

The first indications that these Ni complexes were active electrocatalytically for water reduction were seen in the voltammetric behavior of complex **I** in H_2O/CH_3CN mixtures. Figure 4 displays the reduction behavior of **I** in the absence and presence of water. In the absence of catalyst **I** (Figure 4a, dark blue-dashed curve), there were no indications of enhanced current with added water. The first two reductions of **I** were unchanged with added water and a catalytic current enhancement appears that is associated with the third reduction of the complex (Figures S4 and S5). The shift toward more positive potentials displayed a Nernstian behavior as shown by a linear relationship of the $\log[H_2O]$ against E_{onset} (Figure S23). As we expected, CV measurements with added aqueous phosphate buffer (pH 7) produced a slight increase in current at a given potential (Figure S24). Complex **II** displayed parallel behavior (Figures S23 and S24).

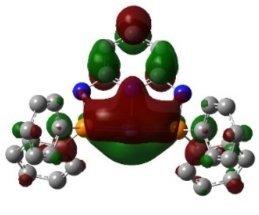

Figure 3. Representation of the SOMO (viewed perpendicular to the molecular plane) obtained from the computational optimization of $[Ni(\kappa^3\text{-}2,6\text{-}\{Ph_2PNH\}_2NC_5H_3)]^-$ (**A**$^-$) using the B3LYP functional and def2TZVP basis set and IEFPCM model for solvation in acetonitrile.

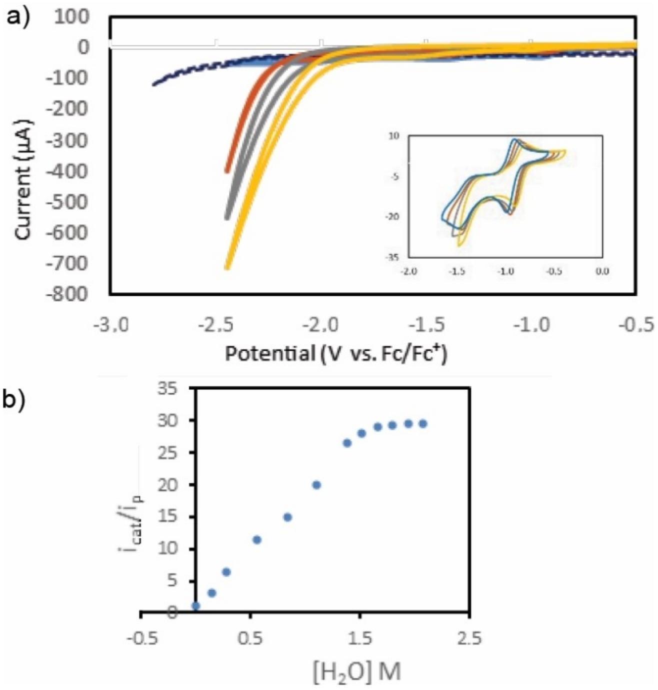

Figure 4. a) Cyclic voltammograms for $[Ni(2,6\text{-}\{Ph_2PNH\}_2(NC_5H_3)Br]^+Br^-$ (**I**; 1.0 mM) under N_2 (light blue) with various amounts of added water (0.28 M = orange, 0.55 M = gray, 1.1 M = yellow) in CH_3CN. Scan rate: 100 mV/s with glassy carbon (GC) working electrode and 0.1 M TBAHFP. Reduction of water in the absence of catalyst is shown in dark blue. Inset: the effect of added water on the first two reductions. b) Plot of the ratio of the catalytic current (i_{cat}) to the peak current of the reduction at −2.55 V in the absence of water (i_p) as a function of the concentration of water.

Linear sweep voltammetry (LSV) measurements substantiated the operationally homogeneous catalytic behavior of **I** and **II** (Figure S25). Repeated scans of a catalyst solution (1 mM Ni complex, 0.5 M water in CH_3CN) gave reproducible catalytic scans. After electrolytic reaction, the electrode was removed, rinsed, and immersed in fresh electrolyte/water solution containing no Ni complex and no catalytic response was observed. Furthermore, a CV of a sample of **I**, previously subjected to bulk electrolysis at −2.55 V against $Fc^{+/0}$ for 1 h, displayed identical reduction peaks of complex **I**. In addition, the difference in catalytic rates of **I** and **II** is consistent with a homogeneous system.

The effect of varying the concentration of added water on the catalytic current, i_c, was also explored. Due to the reduction of solvent, we were not able to achieve a cathodic potential that allowed the observation a maximum catalytic peak current in the data. However, we did measure the increase in i_c relative to the peak current in the absence of water (i_p) at a fixed voltage of −2.55 V (Figure S26). The ratio of i_c to i_p, as a function of $[H_2O]$ is shown in Figure 5. At low concentrations, a linear

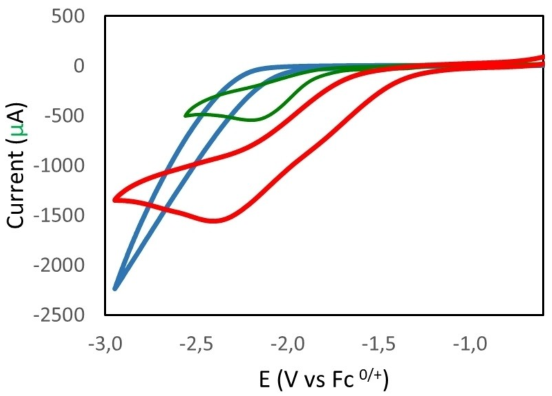

Figure 5. Cyclic voltammograms for $[Ni(2,6\text{-}\{Ph_2PNH\}_2(NC_5H_3)Br]^+Br^-$ (**I**), (1.0 mM) under N_2 in presence of acetic acid in red, phenol in green and water in blue. All substrates 0.55 M in CH_3CN with 0.1 M NBu4PF$_6$, at 100 mV/s using a GC working electrode.

increase in the current ratio was observed with increasing water concentration. When the $[H_2O]$ is sufficiently large that it remains constant, the catalytic current changed from first to zero order as observed in Figure 5. In this substrate concentration-independent region the current ratio can be approximated by Equation (1) with *R* being the ideal gas constant, *T* the absolute temperature, *F* the Faraday constant and *ν* the scan rate used in the cyclic voltammetry measurement in units of V/s.[7,25] As two electrons are used in the formation of H_2, *n* has a value of 2.

$$\frac{i_c}{i_p} = \left(\frac{n}{0.4463}\right)\sqrt{\frac{RTk}{Fv}} \tag{1}$$

This analysis allows the calculation of *k*, a value which represents the number of times a catalyst molecule produces a molecule of H_2 per second, or the turnover frequency (TOF) of this catalyst under these conditions. With a scan rate of 0.1 V/s the saturation current ratio was measured to be 29 giving a TOF for catalyst **I** of 160 s^{-1}.

Quantitative confirmation of H_2 generation was obtained through bulk electrolysis experiments using either **I** or **II** as a catalyst for generating H_2 from H_2O/CH_3CN at −2.55 V versus $Fc^{+/0}$ with a glassy carbon electrode having a surface area of 1.38 cm^2. The reaction head-space was analyzed by GC and confirmed dihydrogen evolution with 88 % Faradaic efficiency (Table S14, Figure S27).

As part of our continuing investigation of this catalyst system we explored the effect of changing the substrate for catalytic H_2 generation. The ability to employ either phenol or acetic acid as substrates was confirmed through appearance of catalytic currents in the presence of catalysts **I** and **II** as shown in Figure 5 (Figure S28). As expected, the catalytic onset potential and current correlated with pK_a values of phenol (**I**, $E_{onset} = -1.7$ V; $E_{cat/2} = -1.95$ V; $pK_a = 29.14$) and acetic acid (**I**, $E_{onset} = -1.25$ V; $E_{cat/2} = -1.83$ V; $pK_a = 23.51$) in acetonitrile.[26] The overpotential for reduction of these substrates can be calculated using Equations (2) and (3).[27,28] With catalyst **I**, the overpotentials were 200 and 410 mV for phenol and acetic acid, respectively.

$$\text{overpotential} = \eta = E_{cat/2} - E_{H^+} \tag{2}$$

$$E_{H}^{+} = -0.028\,V - 0.05916\,V \times pK_a \tag{3}$$

These reductions appear to correlate most closely with the second reduction of the Ni complex and suggest that these substrates follow a more conventional $Ni^{II/0}$ mechanism for H_2 generation.

Experimental and computational data point to a key role for the ligand in any proposed mechanism for the electrocatalytic generation of H_2 from water using either Ni complex **I** or **II**. The redox activity of this class of pincer ligands and their ability to undergo one electron transfer with first row metals is an open question in the literature.[29,30] A CV measurement of the ligands in CH_3CN using a glassy carbon (GC) working electrode did display an irreversible reductions at approximately −2.55 V against $Fc^{+/0}$ (Figure S29). Importantly, bulk electrolysis measurements with the ligands did not produce any measurable hydrogen gas.

A proposed mechanism for the catalytic behavior of these Ni complexes is summarized in Figure 6. For simplicity, the scheme is presented and discussed based on **I** but is entirely analogous for **II**. Hydrogen formation is correlated with the reduction at −2.55 V and computations have identified this species as a d^{10} Ni^{0I} species with an anionic ligand, **A**⁻. A first step in hydrogen formation is likely a proton transfer from H_2O to **A**⁻. In order to explore the structure of this proposed species,

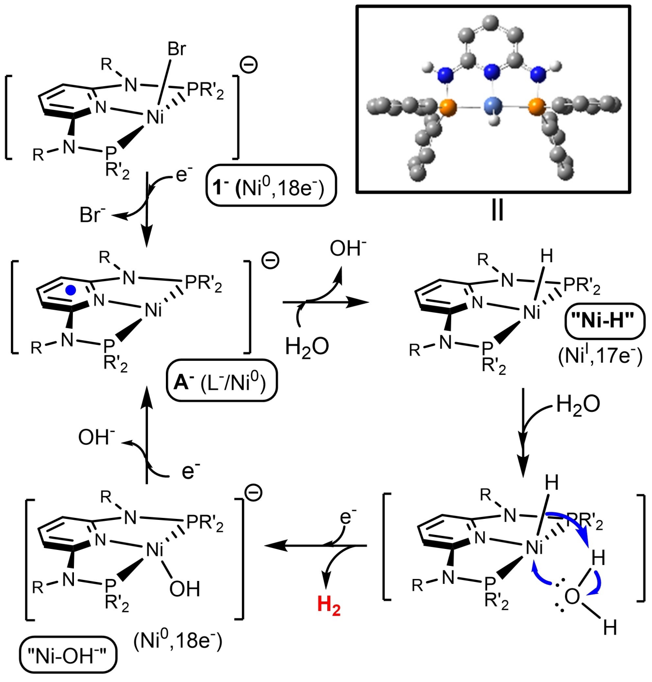

Figure 6. Proposed mechanism for the reduction of water and formation of H_2 from complex $[Ni(\kappa^3\text{-}2,6\text{-}\{Ph_2PNH\}_2NC_5H_3)]^-$ (**A**⁻). Inset is the optimized (DFT, B3LYP, def2TZVP) structure of Ni–H.

a set of DFT (B3LYP/def2TZVP/IEPCM) optimizations were carried out for the addition of a proton to several locations in $\mathbf{A}^-$. The lowest energy species corresponded to loss of one electron each from the ligand anion and Ni^{0I} and the formation of a Ni^{I} hydride, "Ni–H" shown as the inset in Figure 6 (Figures S32 and S33, Table S15) Reaction of this complex with water would lead to hydrogen release and formation of a Ni^{0I} complex ("$Ni–OH^-$") under the reducing conditions employed for the reaction. This intermediate species is the analogue of the Ni^{0I} complex $\mathbf{1}^-$ and was computationally optimized (Figure S34, Table S16). In analogy to $\mathbf{1}^-$, $Ni–OH^-$ could undergo reduction with hydroxide loss to return to $\mathbf{A}^-$ and close the catalytic cycle.

In order to bring electrocatalytic hydrogen production into the sustainable realm, earth abundant metal catalysts should function with water as the substrate. These newly reported hydrogen generating catalysts of Ni^{II} are robust, air stable and electrocatalytically reduce water to hydrogen with excellent Faradaic efficiency. Computations supplemented our understanding of a unique ligand-based electron transfer with the cooperativity of the PN^3P ligand as an electron reservoir as a requirement for successful catalysis.

The framework of these catalysts is amenable to ligand variations and we continue to explore suitable ligand modifications to tune catalyst performance, reduce reduction potentials and improve solubility in water. Extended studies including elucidation of the mechanism by DFT are in progress. These results inspire the synthesis and characterization of new compounds that will both provide insight into the mechanisms of and replace precious metal catalysts in hydrogen production and application.

Deposition Numbers 2098674 (**I**) and 2098675 (**II**) contain the supplementary crystallographic data for this paper. These data are provided free of charge by the joint Cambridge Crystallographic Data Centre and Fachinformationszentrum Karlsruhe Access Structures service.

Conflict of Interest

The authors declare no conflict of interest.

Keywords: Electrocatalysis · hydrogen production · nickel · reduction of water

[1] B. Fisher, R. Eisenberg, *J. Am. Chem. Soc.* **1980**, *102*, 7361–7363.
[2] M. Wang, L. Chen, L. Sun, *Energy Environ. Sci.* **2012**, *5*, 6763–6778.
[3] V. S. Thoi, Y. Sun, J. R. Long, C. J. Chang, *Chem. Soc. Rev.* **2013**, *42*, 2388–2400.
[4] J. W. Wang, W. J. Liu, D. C. Zhong, T. B. Lu, *Coord. Chem. Rev.* **2019**, *378*, 237–261.
[5] G. Luo, H. Zhang, Y. Tao, Q. Wu, *Inorg. Chem. Front.* **2019**, *6*, 343–354.
[6] B. L. Greene, C. H. Wu, G. E. Vansuch, M. W. W. Adams, R. B. Dyer, *Biochemistry* **2016**, *55*, 1813–1825.
[7] M. L. Helm, M. P. Stewart, R. M. Bullock, M. R. Dubois, D. L. Dubois, *Science* **2011**, *333*, 863–866.
[8] M. R. Dubois, D. L. Dubois, *Acc. Chem. Res.* **2009**, *42*, 1974–1982.
[9] P. H. A. Kankanamalage, S. Mazumder, V. Tiwari, K. K. Kpogo, H. Bernhard Schlegel, C. N. Verani, *Chem. Commun.* **2016**, *52*, 13357–13360.
[10] K. Koshiba, K. Yamauchi, K. Sakai, *Angew. Chem. Int. Ed.* **2017**, *56*, 4247–4251; *Angew. Chem.* **2017**, *129*, 4311–4315.
[11] L. Gan, T. L. Groy, P. Tarakeshwar, S. K. S. Mazinani, J. Shearer, V. Mujica, A. K. Jones, *J. Am. Chem. Soc.* **2015**, *137*, 1109–1115.
[12] B. H. Solis, A. G. Maher, D. K. Dogutan, D. G. Nocera, S. Hammes-Schiffer, *Proc. Nat. Acad. Sci.* **2016**, *113*, 485–492.
[13] A. Z. Haddad, B. D. Garabato, P. M. Kozlowski, R. M. Buchanan, C. A. Grapperhaus, *J. Am. Chem. Soc.* **2016**, *138*, 7844–7847.
[14] S. P. Cronin, A. Al Mamun, M. J. Toda, M. S. Mashuta, Y. Losovyj, P. M. Kozlowski, R. M. Buchanan, C. A. Grapperhaus, *Inorg. Chem.* **2019**, *58*, 12986–12997.
[15] L. Chen, X. Li, G. Ren, P. Zhang, N. Wang, *ChemCatChem* **2020**, *12*, 3853–3856.
[16] P. Zhang, M. Wang, Y. Yang, D. Zheng, K. Han, L. Sun, *Chem. Commun.* **2014**, *50*, 14153–14156.
[17] H. Li, B. Zheng, K.-W. Huang, *Coord. Chem. Rev.* **2015**, *293–294*, 116–138.
[18] H. Li, T. P. Goncalves, Q. Zhao, D. Gong, Z. Lai, Z. Wang, J. Zheng, K. Huang, *Chem. Commun.* **2018**, *54*, 11395.
[19] H. Li, J. Hu, Q. Zhao, D. Gong, Z. Lai, Z. Wang, J. Zheng, K. Huang, *J. Org. Chem.* **2018**, *83*, 14969–14977.
[20] D. Lupp, K. W. Huang, *Organometallics* **2020**, *39*, 18–24.
[21] G. K. Rao, W. Pell, B. Gabidullin, I. Korobkov, D. Richeson, *Chem. A Eur. J.* **2017**, *23*, 16763–16767.
[22] W. Schirmer, U. Florke, H.-J. Haupt, *Z. Anorg. Allg. Chem.* **1987**, *545*, 83–97.
[23] D. Benito-Garagorri, E. Becker, J. Wiedermann, W. Lackner, M. Pollak, K. Mereiter, J. Kisala, K. Kirchner, *Organometallics* **2006**, *25*, 1900–1913.
[24] M. Mastalir, E. Pittenauer, K. Kirchner, *Org. Lett.* **2016**, 3186–3189.
[25] D. H. Pool, D. L. Dubois, *J. Organomet. Chem.* **2009**, *694*, 2858–2865.
[26] A. Kutt, I. Leito, I. Kaljurand, L. Soovali, V. M. Vlasov, L. M. Yagupolski, I. A. Koppel, *J. Org. Chem.* **2006**, *71*, 2829–2838.
[27] A. M. Appel, M. L. Helm, *ACS Catal.* **2014**, *4*, 630–633.
[28] B. D. McCarthy, D. J. Martin, E. S. Rountree, A. C. Ullman, J. L. Dempsey, *Inorg. Chem.* **2014**, *53*, 8350–61.
[29] D. W. Shaffer, I. Bhowmick, A. L. Rheingold, C. Tsay, B. N. Livesay, M. P. Shores, J. Y. Yang, *Dalton Trans.* **2016**, *45*, 17910–17917.
[30] S. P. Semproni, C. Milsmann, P. J. Chirik, *J. Am. Chem. Soc.* **2014**, *136*, 9211.

Manuscript received: June 9, 2021
Version of record online: ■■■, ■■■

COMMUNICATION

Towards sustainable H_2 production: To bring electrocatalytic hydrogen production into the sustainable realm, earth-abundant metal catalysts should function with water as the substrate. These newly reported hydrogen-generating catalysts of Ni^{II} are robust, stable in air and electrocatalytically reduce water to hydrogen with excellent Faradaic efficiency. Computations supplemented our understanding of a unique ligand-based electron transfer with the cooperativity of the PN^3P ligand as an electron reservoir as a requirement for successful catalysis.

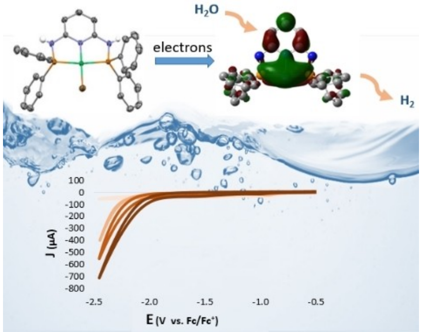

*S. Norouziyanlakvan, Dr. G. K. Rao, Dr. J. Ovens, Dr. B. Gabidullin, Dr. D. Richeson**

1 – 6

Electrocatalytic H_2 Generation from Water Relying on Cooperative Ligand Electron Transfer in "PN^3P" Pincer-Supported Ni^{II} Complexes